Title
Ozone and alkyl nitrate formation from the Deepwater Horizon oil spill atmospheric emissions

Journal
Journal of Geophysical Research Atmospheres, 117(9)

ISSN
0148-0227

Authors
Neuman, JA
Aikin, KC
Atlas, EL
et al.

Publication Date
2012

DOI
10.1029/2011JD017150

Ozone and alkyl nitrate formation from the Deepwater Horizon oil spill atmospheric emissions

J. A. Neuman,[1,2] K. C. Aikin,[1,2] E. L. Atlas,[3] D. R. Blake,[4] J. S. Holloway,[1,2] S. Meinardi,[4] J. B. Nowak,[1,2] D. D. Parrish,[2] J. Peischl,[1,2] A. E. Perring,[1,2] I. B. Pollack,[1,2] J. M. Roberts,[2] T. B. Ryerson,[2] and M. Trainer[2]

Received 9 November 2011; revised 6 April 2012; accepted 9 April 2012; published 11 May 2012.

[1] Ozone (O_3), alkyl nitrates ($RONO_2$), and other photochemical products were formed in the atmosphere downwind from the Deepwater Horizon (DWH) oil spill by photochemical reactions of evaporating hydrocarbons with NOx (=NO + NO_2) emissions from spill response activities. Reactive nitrogen species and volatile organic compounds (VOCs) were measured from an instrumented aircraft during daytime flights in the marine boundary layer downwind from the area of surfacing oil. A unique VOC mixture, where alkanes dominated the hydroxyl radical (OH) loss rate, was emitted into a clean marine environment, enabling a focused examination of O_3 and $RONO_2$ formation processes. In the atmospheric plume from DWH, the OH loss rate, an indicator of potential O_3 formation, was large and dominated by alkanes with between 5 and 10 carbons per molecule (C_5–C_{10}). Observations showed that NOx was oxidized very rapidly with a 0.8 h lifetime, producing primarily C_6–C_{10} $RONO_2$ that accounted for 78% of the reactive nitrogen enhancements in the atmospheric plume 2.5 h downwind from DWH. Both observations and calculations of $RONO_2$ and O_3 production rates show that alkane oxidation dominated O_3 formation chemistry in the plume. Rapid and nearly complete oxidation of NOx to $RONO_2$ effectively terminated O_3 production, with O_3 formation yields of 6.0 ± 0.5 ppbv O_3 per ppbv of NOx oxidized. VOC mixing ratios were in large excess of NOx, and additional NOx would have formed additional O_3 in this plume. Analysis of measurements of VOCs, O_3, and reactive nitrogen species and calculations of O_3 and $RONO_2$ production rates demonstrate that NOx-VOC chemistry in the DWH plume is explained by known mechanisms.

Citation: Neuman, J. A., et al. (2012), Ozone and alkyl nitrate formation from the Deepwater Horizon oil spill atmospheric emissions, *J. Geophys. Res.*, *117*, D09305, doi:10.1029/2011JD017150.

1. Introduction

[2] Tropospheric ozone (O_3) production caused by photochemical reactions between NOx (=NO + NO_2) and volatile organic compounds (VOCs) has been studied extensively in urban, industrial, and rural environments [*National Research Council Committee on Tropospheric Ozone Formation and Measurement*, 1991]. VOCs react with the hydroxyl radical (OH) to produce peroxy radicals (RO_2 and HO_2) that rapidly convert NO to NO_2. Subsequent photolysis of NO_2 produces an oxygen atom that combines with molecular oxygen to form O_3. Since NO_2 photolysis also produces NO, the process can cycle until NOx is further oxidized, terminating the catalytic O_3 formation cycle.

[3] The initial VOC mixture and ratio to NOx determines the effective catalytic chain length. Alkene oxidation can form relatively reactive secondary species such as aldehydes and peroxyacyl nitrates ($RC(O)O_2NO_2$) that propagate the O_3 formation cycle. In contrast, alkane oxidation forms less reactive secondary NOx oxidation products and VOCs, primarily monofunctional alkyl nitrates ($RONO_2$) and ketones, which effectively terminate O_3 production [*Carter*, 1994]. Source characterization and photochemical processes in transported air masses have been analyzed by examining $RONO_2$ formation from anthropogenic emissions of alkane precursors [*Simpson et al.*, 2003; *Madronich*, 2006; *Simpson et al.*, 2006; *Reeves et al.*, 2007; *Worton et al.*, 2010]. Investigating these known processes in an environment with a unique VOC mixture provides a new opportunity to test our understanding of photochemical formation of O_3 and other secondary products.

[1]Cooperative Institute for Research in Environmental Sciences, University of Colorado Boulder, Boulder, Colorado, USA.
[2]Chemical Sciences Division, Earth System Research Laboratory, NOAA, Boulder, Colorado, USA.
[3]Rosenstiel School of Marine and Atmospheric Science, University of Miami, Miami, Florida, USA.
[4]Department of Chemistry, University of California, Irvine, California, USA.

Corresponding author: A. Neuman, Cooperative Institute for Research in Environmental Sciences, University of Colorado Boulder, 325 Broadway, Boulder, CO 80305, USA. (andy.neuman@noaa.gov)

0148-0227/12/2011JD017150

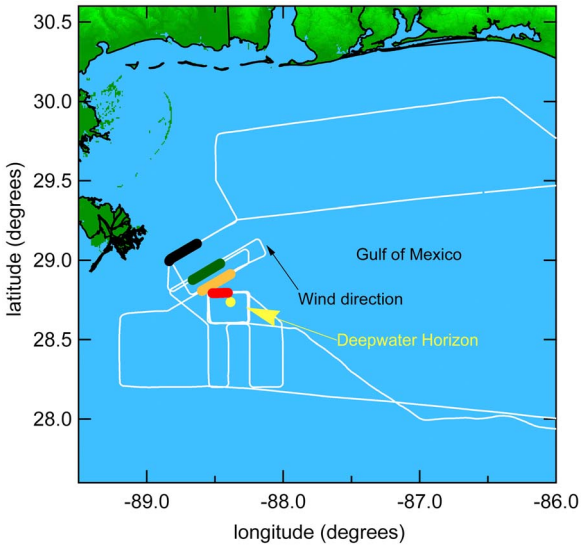

Figure 1. Map of the WP-3D flight track (white line) over the Gulf of Mexico on 10 June 2010. The yellow circle marks the location of the DWH oil platform. The aircraft sampled plumes in the atmospheric MBL at four distances downwind from DWH indicated by the thick bars: 10 km (red), 20 km (orange), 30 km (green), and 50 km (black).

[4] On 20 April 2010, an explosion and fire destroyed the Deepwater Horizon (DWH) offshore oil platform. For the ensuing three months, oil leaked from the wellhead at the seafloor, 1520 m below the surface in the Gulf of Mexico. Large amounts of oil from the DWH spill reached the ocean surface and promptly evaporated [*Ryerson et al.*, 2011]. Measurements in and over the ocean showed that little methane [*Yvon-Lewis et al.*, 2011] and other light alkanes [*Ryerson et al.*, 2011] were released to the atmosphere, since they nearly fully dissolved in the seawater. The unique speciation of the VOC mixture released to the atmosphere from this deep-water oil spill provided a new environment for examination of tropospheric photochemistry [e.g., *de Gouw et al.*, 2011], particularly that initiated by OH oxidation of relatively heavy alkanes. Such a large emission of VOCs into a remote marine environment enabled a study of secondary photochemical products without the confounding influences of a multitude of sources [*Neuman et al.*, 2009] and broad mix of VOCs typically found over the continent. Spill response efforts emitted NOx from ship exhaust, surface oil burning, and flaring of recovered gas into the atmosphere in the vicinity of the oil spill. The subsequent gas-phase photochemical reactions between NOx and hydrocarbons evaporating from the surface oil slick are studied in the downwind plume from DWH. In particular, O_3 and the $RONO_2$ oxidation products formed from reactions between these NOx and VOC emissions are examined in detail.

2. Measurements

[5] The National Oceanic and Atmospheric Administration (NOAA) WP-3D instrumented aircraft flew over the Gulf of Mexico in the vicinity of DWH on 8 and 10 June 2010. The aircraft sampled the plume of DWH emissions during the daytime at altitudes between 60 and 200 m above the sea surface and well within the well-mixed marine boundary layer (MBL) that was approximately 600 m deep [*Ryerson et al.*, 2011]. Figure 1 shows a map of the region and the flight track of the aircraft on 10 June 2010. The gas-phase species studied here were emitted from a small area and remained confined to a narrow plume, spreading less than 10 km horizontally at 50 km downwind. On 10 June, the winds in the MBL were steady out of the southeast at 5.7 ± 0.4 m/s [*Ryerson et al.*, 2011, auxiliary material] at the locations and times that the WP-3D sampled the DWH plume. The colored portions of the flight track in Figure 1 indicate four locations at 10, 20, 30, and 50 km downwind from DWH where the plume was repeatedly sampled to capture chemical transformations during transport. Atmospheric transport times calculated from the average wind speed and the distance from DWH to the plume sampling locations were approximately 0.5, 1.0, 1.5, and 2.5 h in the four transects shown in Figure 1.

[6] This analysis uses fast-response in situ measurements of reactive nitrogen species, O_3, and meteorological parameters, and measurements of VOCs and $RONO_2$ in whole air canister samples. All data are publicly available at http://esrl.noaa.gov/csd/tropchem/2010gulf/. Independent chemical ionization mass spectrometer instruments measured nitric acid (HNO_3) [*Neuman et al.*, 2002] and peroxyacetyl nitrate (PAN; $CH_3C(O)O_2NO_2$), [*Slusher et al.*, 2004] with uncertainties of ±(15% + 0.040 ppbv) and ±(20% + 0.005 ppbv), respectively. NO, NO_2, NOy (=NO + NO_2 + PAN + HNO_3 + $RONO_2$ + …) and O_3 measured by chemiluminescence were reported once per second with uncertainties of ±(3% + 0.01 ppbv), ±(4% + 0.03 ppbv), ±(12% + 0.10) ppbv, and ±(2% + 0.015 ppbv), respectively [*Ryerson et al.*, 1998, 1999; *Pollack et al.*, 2011]. Carbon monoxide (CO) was measured with 5% uncertainty by vacuum ultraviolet fluorescence [*Holloway et al.*, 2000], and methane (CH_4) was measured by cavity ringdown spectroscopy [*Chen et al.*, 2010]. Speciated VOCs and $RONO_2$ were determined by gas chromatography with flame ionization or mass spectrometric analysis of 72 whole air samples collected in stainless steel canisters on each flight [*Colman et al.*, 2001]. Each canister was filled in approximately 4 s and the sampling was manually initiated to target the plume from DWH. Eight $RONO_2$ compounds with between one and five carbon atoms per molecule were measured with ±10% accuracy, and in a few samples the sum of C_6–C_8 $RONO_2$ were estimated with approximately ±50% uncertainty (D. R. Blake, personal communication, 2011). The estimates of the C_6–C_8 $RONO_2$ mixing ratios were made by assuming all chromatogram peaks that appeared at retention times larger than the pentyl nitrates were heavier alkyl nitrates, and that the detector response for the heavier alkyl nitrates was the same as for the lighter nitrates. Since longer chain (>C_8) $RONO_2$ were likely lost in the analytical system, C_9–C_{11} $RONO_2$ were not measured here. VOCs measured in the canisters include aromatics, alkenes, and 27 linear and branched alkanes with up to 11 carbons per molecule (C_{11}) [*Ryerson et al.*, 2011]. Accuracies for the VOCs analyzed here were typically ±10%.

3. Results

[7] Only the 10 June results are analyzed in detail below, since transport times could not be determined unambiguously

Table 1. Trace Gas Mixing Ratios Measured on 10 June 2010 in the MBL Below 0.2 km Altitude Over the Gulf of Mexico in Two Plumes From DWH and Upwind of DWH[a]

Species	10 km Downwind (ppbv)	50 km Downwind (ppbv)	Upwind (ppbv)
NOy	9.3	2.7	0.6
NO_2	4.8	0.12	0.01
CO	139	140	133
methane/1000	1888	1887	1882
ethane	1.4	1.2	1.1
propane	2.7	0.8	0.164
n-butane	21.7	4.9	0.020
n-pentane	29.8	7.4	0.009
n-hexane	25.1	6.7	0.008
methylcyclohexane	25.4	6.6	0.009
n-octane	15.3	4.2	0.011
n-nonane	13.2	3.9	0.012
n-decane	8.8	3.0	0.012
m+p xylene	7.3	1.2	<0.003
1,2,4 trimethylbenzene	3.5	0.6	<0.003

[a]Two plumes from DWH are shown in Figure 4. Only the most abundant alkane and aromatic isomers are listed.

under the light and variable winds that prevailed during the 8 June flight. However, the enhancement ratios of trace gases were similar on the 8 June and 10 June flights, suggesting that the findings are representative of photochemical processing in the DWH plume.

3.1. Atmospheric VOC Abundance

[8] Downwind from DWH, the mixture of atmospheric VOCs from evaporating surface oil was markedly different from VOC mixtures in other urban, industrial, and remote environments that have been investigated. Upwind from DWH, background concentrations of C_5–C_{10} alkanes in the Gulf of Mexico MBL were less than 20 pptv (Table 1), consistent with measurements from a research vessel in 2006 in the same region [*Gilman et al.*, 2009]. In the DWH plumes measured here, many C_5–C_{10} alkanes exceeded 10 ppbv (Table 1), and were considerably more abundant than generally found in U.S. urban and industrial areas [*Baker et al.*, 2008; *Jobson et al.*, 2004]. Furthermore, the mass flux of the measured VOCs in the DWH plumes was independent (within approximately 50% uncertainties) of downwind distance [*Ryerson et al.*, 2011, Figure 3a], indicating negligible VOC loss within the transport times examined here. In highly concentrated urban and petrochemical industrial plumes sampled near Houston, Texas, peak C_5–C_{10} alkane mixing ratios were similar to the levels measured here [*Gilman et al.*, 2009; *Ryerson et al.*, 2003; *Washenfelder et al.*, 2010]; however, C_2–C_4 alkanes and alkenes were even more abundant than the C_5–C_{10} alkanes in the Houston plumes. VOC speciation in the DWH plume was characterized by extremely high concentrations of C_5–C_{10} alkanes without corresponding enhancements in lighter alkanes or alkenes. Heavier aromatics also were present in the atmospheric DWH plumes at ppbv-levels (Table 1), whereas lighter aromatics such as benzene and toluene were not substantially enhanced because they were efficiently dissolved in the ocean [*Ryerson et al.*, 2011].

3.2. Contributions to OH Loss Rate

[9] Measurements of VOCs and other trace gases downwind of DWH are used to calculate OH loss rates, which are the product of a compound's concentration with its rate coefficient for reaction with OH (k_{OH}). O_3 formation is favored when VOCs that propagate photochemical reactions dominate the OH loss rate, while O_3 formation is inhibited when compounds that form unreactive secondary products dominate the OH loss rate. For example, a large OH loss rate from NO_2 suppresses O_3 formation, because NO_2 reacts with OH to form HNO_3. Since HNO_3 formation removes NOx and OH radicals from rapid photochemical reactions [*Neuman et al.*, 2006], it can represent a terminating step in O_3 formation photochemistry.

[10] The OH loss rate of compounds measured in the DWH plume over the Gulf of Mexico was dominated by C_5–C_{10} alkanes and C_8–C_9 aromatics. Figure 2 compares OH loss rates for alkanes and aromatics measured in a plume 10 km downwind from DWH to similar measurements in freshly emitted urban and petrochemical plumes. The great abundance of these alkanes in all plume transects (ranging from 0.5 to 2.5 h downwind) caused the OH loss rate from the sum of the measured C_5–C_{10} alkanes to exceed 10 s^{-1} in all DWH plume transects, with the greatest contributions from several C_7 alkanes. The OH loss rate from aromatics was dominated by C_9 molecules and was less than a fourth the loss rate from alkanes. Alkane mixing ratios greatly exceeded alkene mixing ratios, such that the OH loss rate from total alkenes was negligible even though alkenes have larger k_{OH}. In contrast, in plumes influenced by Houston petrochemical emissions, alkenes with large k_{OH} dominated the OH loss rate (Figure 2), even though they were not the most abundant VOCs [*Ryerson et al.*, 2003; *Washenfelder et al.*, 2010]. NO_2 levels in the DWH plume (Table 1) were much less than found in many urban locations, where the OH loss rate can be dominated by NO_2 (e.g., the Dallas plume, Figure 2). The OH loss rate from NO_2 was less than 1 s^{-1} even in the closest DWH plume transects with the highest NO_2 concentrations. CO and CH_4 in the DWH plume were not substantially enhanced above background, and OH loss rates from these compounds were less than 1 s^{-1}, similar to that in the upwind marine atmosphere. In summary, the emission plume from DWH represents a unique chemical regime where high OH loss rates were dominated by C_5–C_{10} alkanes, while NO_2, CO, CH_4, and alkenes made relatively small contributions to the OH loss rate. The effects on NOx oxidation and O_3 formation rates and yields are examined below.

3.3. NOx Oxidation Rate

[11] In the MBL near DWH, NOx emissions from ships, flaring of recovered gas, and other response operations mixed with VOCs evaporating from the surfaced oil. On 10 June, peak NOx mixing ratios of 10 ppbv from these recovery operations were 2–3 orders of magnitude greater than the 20–50 pptv background NOx outside the plume (Table 1).

[12] NOy is a measurement of NOx and its oxidation products [*Fahey et al.*, 1986]. NOy is a conserved tracer of NOx emissions, assuming negligible loss of reactive nitrogen species, which is a good approximation on these short

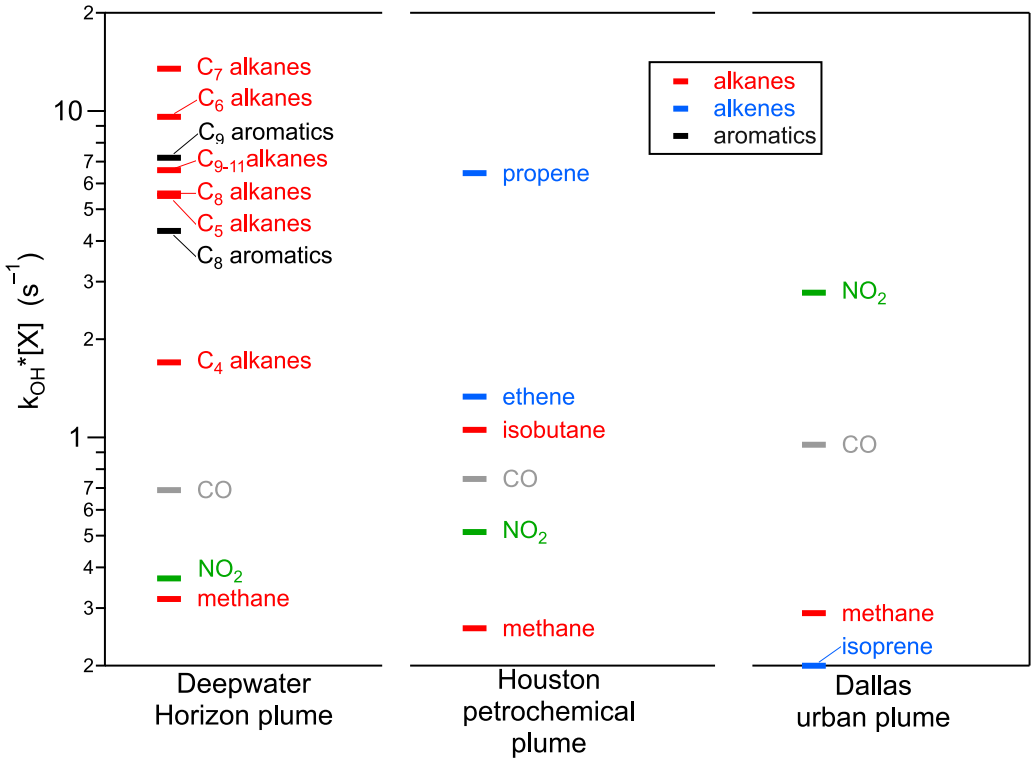

Figure 2. OH loss rates greater than 0.2 s^{-1} in a plume 10 km downwind from DWH plume on 10 June 2010 (shown in Figure 4a and Table 1), compared to OH loss rates in a plume downwind from Houston petrochemical industrial emissions [*Ryerson et al.*, 2003] and over the Dallas urban area on 25 September 2006. The individually measured compounds that contributed to the carbon number groupings in the DWH plume are: C_4 alkanes = isobutane + n-butane, C_5 alkanes = isopentane + n-pentane + cyclopentane, C_6 alkanes = n-hexane + cyclohexane + 2-methylpentane + 3-methylpentane + methylcyclopentane, C_7 alkanes = n-heptane + 2-methylhexane + 3-methylhexane + methylcyclohexane, C_8 alkanes = n-octane + 2-methylheptane, $C_{9–11}$ alkanes = n-nonane + n-decane + undecane, C_8 aromatics = ethylbenzene + m, o, and p-xylenes, C_9 aromatics = 1,2,3-trimethylbenzene + 1,3,5-trimethylbenzene + 1,2,4-trimethylbenzene + n-propylbenzene + 3-ethyltoluene + 4-ethyltoluene.

time scales (≤2.5 h). Reactive nitrogen is emitted from combustion sources primarily as NO, and the ratio of plume NOx to NOy (NOx:NOy) approaches unity at the time of emission. NOx:NOy decreases over time as NOx is oxidized to other NOy species during transport downwind, and the change in the ratio quantifies NOx oxidation in the plume. NOx and NOy were highly correlated in the DWH plume transects, with $r^2 > 0.97$ in all but the most aged plumes, where $r^2 = 0.84$. NOx:NOy, determined from linear least squares fits to the data from each crosswind plume transect, versus plume transport time is shown in Figure 3a. Ten km downwind from DWH, NOx:NOy was 0.817 ± 0.005 ppbv/ppbv, indicating that almost 20% of the emitted NOx already had been oxidized in these plumes that had aged only 0.5 h since emission. NOx:NOy decreased rapidly with further plume transport, reaching 0.06 at 2.5 h and 50 km downwind. The NOx photochemical lifetime, determined from a linear least squares fit of the logarithm of NOx:NOy measured in each plume transect versus transport time, was unusually short at 0.83 ± 0.16 h (solid line in Figure 3a). NOx loss by OH + NO_2 was negligible here, as demonstrated by the absence of HNO_3 production in the plumes (Figure 4). Instead, the rapid NOx loss was caused by the reaction of peroxy radicals with NO (discussed in section 3.5 below). In comparison, NOx lifetimes in power plant plumes were 6 h [*Ryerson et al.*, 1998], and those in VOC-rich plumes from Houston petrochemical industrial sources were 1.8 h (dashed line, Figure 3a) [*Ryerson et al.*, 2003]. The extremely rapid decrease of NOx:NOy downwind from DWH shows that the chemistry was prompt with essentially complete NOx oxidation within three hours.

3.4. NOx Oxidation Products

[13] The secondary oxidation products from NOx-VOC photochemistry reveal the atmospheric processes responsible for the rapid NOx oxidation. Figure 4 illustrates temporal changes in reactive nitrogen partitioning in the DWH plume. In fresh plumes (e.g., Figure 4a), NOx accounted for over 80% of plume NOy. In aged plumes (e.g., Figure 4b), NOx oxidation was nearly complete, but NOx, PAN, HNO_3, and the sum of eight C_1–C_5 $RONO_2$ accounted for only 22% of plume NOy. This result differs dramatically from previous studies, where the sum of NOx + PAN + HNO_3 accounted for over 96% of NOy in urban and petrochemical plumes [*Neuman et al.*, 2002; *Ryerson et al.*, 2003] and for approximately 90% of NOy in rural areas [*Parrish et al.*, 1993]. In urban air masses, $RONO_2$ often accounted for a few percent of NOy [*O'Brien et al.*, 1997; *Flocke et al.*,

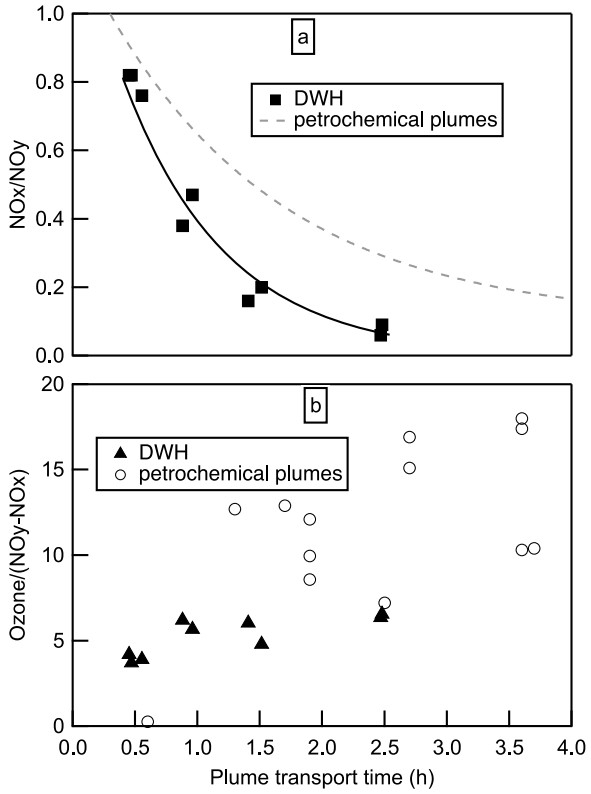

Figure 3. (a) NOx to NOy enhancement ratios measured in nine DWH plume transects versus downwind transport time. The solid line is a fit to the data. (b) The ozone production efficiency (OPE) determined from the ratio of O_3 to NOy−NOx measured in the same plume transects are shown as closed triangles. For comparison, NOx lifetimes (dashed line in Figure 3a) and OPE in Houston petrochemical industrial plumes (open circles in Figure 3b) from *Ryerson et al.* [2003] are shown.

1998; *Schneider et al.*, 1998; *Talbot et al.*, 2003; *Ryerson et al.*, 2003], and up to 10–20% of NOy in some studies [*Day et al.*, 2003; *Perring et al.*, 2010].

[14] The NOx oxidation products that account for the majority of NOy in the aged plumes were not measured directly here, but they can be inferred from the measurements. Although heavier $RONO_2$ were not reported regularly from the whole air samples, C_6–C_8 $RONO_2$ were measured with approximately 50% uncertainty in selected canisters in DWH plumes [described in section 2 above]. For example, near the center of the plume 50 km and 2.5 h downwind from DWH (Figure 4b), most NOx was oxidized and PAN and HNO_3 formation was small. Where the canister was sampled closest to the plume center, the difference between NOy and ($NOx + PAN + HNO_3$) was approximately 1 ppbv. The C_1–C_5 $RONO_2$ were enhanced by 60 pptv, and the C_6–C_8 $RONO_2$ were enhanced by several hundred pptv (not shown). Although >C_8 $RONO_2$ were not measured here, their mixing ratios are expected to be substantially increased since their production rate from the measured parent alkanes is calculated to be large [section 3.5]. The large difference between NOy and the sum of the individually measured compounds was only apparent in aged DWH plumes. Although all alkyl nitrates are not measured here, the observations are consistent with $RONO_2$ species with more than 5 carbon atoms accounting for the majority of reactive nitrogen in aged DWH plumes.

3.5. Alkyl Nitrate Production Estimated From VOC Measurements

[15] The presence of long chain $RONO_2$ in aged DWH plumes suggested by the NOy difference measurements is supported by calculations of $RONO_2$ abundance and speciation in the DWH plume using measurements of the parent

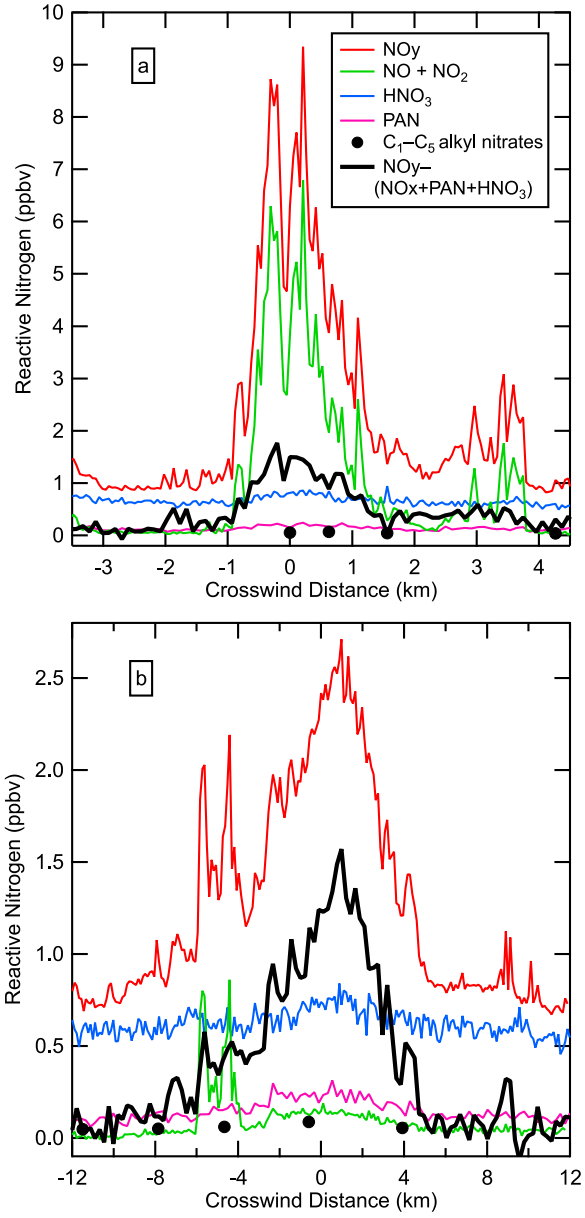

Figure 4. Time series of reactive nitrogen species measured on 10 June 2010 in the MBL in plumes (a) 10 km and (b) 50 km downwind from DWH. NOx, NOy, and HNO_3 were measured once per s and PAN was measured once per 2 s. C_1–C_5 alkyl nitrates were measured in whole air samples at locations indicated by the circles. The sum of alkyl nitrates (black lines) is inferred from the difference between NOy and ($NOx + PAN + HNO_3$).

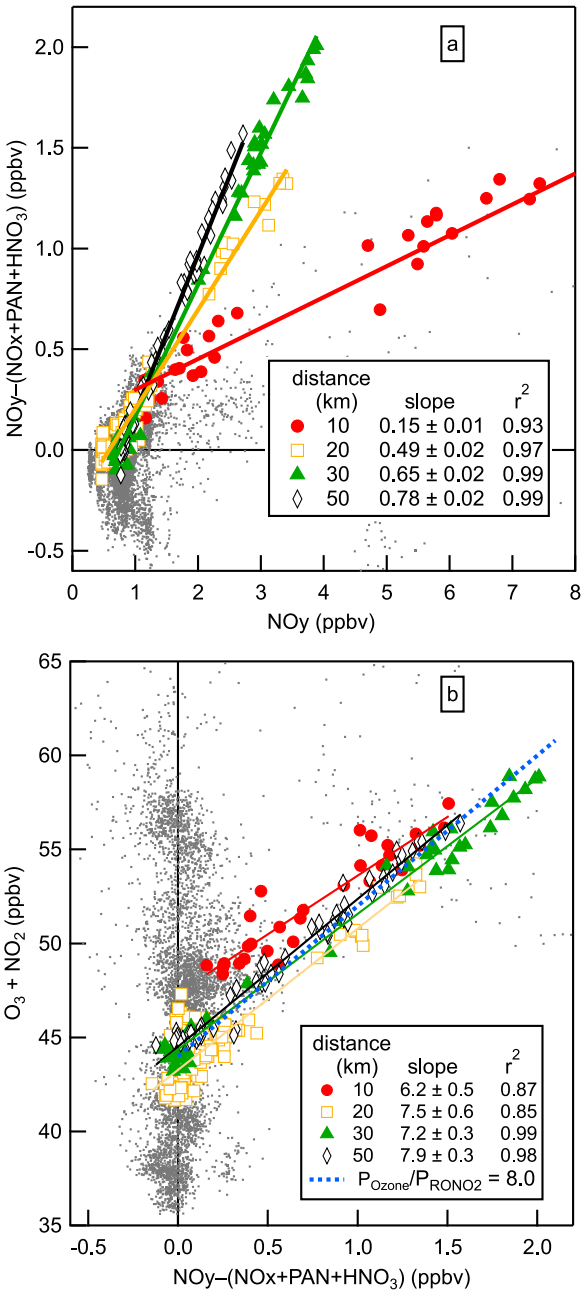

Figure 5. The 1-s measurements of (a) NOy − (NOx + PAN + HNO_3) versus NOy (gray dots) and (b) O_3 + NO_2 versus NOy − (NOx + PAN + HNO_3) (gray dots) over the Gulf of Mexico on the 10 June 2010 WP-3D flight. Colored symbols indicate measurements in four plume transects 10 km (red), 20 km (orange), 30 km (green), and 50 km (black) downwind from DWH. Lines through the colored points are the linear least squares fits to the data from a single plume transect. The correlation slope for each line is shown with 95% confidence intervals. The blue dashed line in Figure 5b is the calculated ratio of O_3 to $RONO_2$ production rates from section 3.6.

alkanes. The $RONO_2$ production rate (P_{RONO_2}) from each parent VOC is determined from the measured VOC concentration, k_{OH} for that VOC, and the branching ratio for $RONO_2$ formation (β) from the reaction of the product RO_2 with NO [*Atkinson et al.*, 1982; *Roberts*, 1990; *Arey et al.*, 2001; *Perring et al.*, 2010] as

$$P_{RONO_2} = \beta \times k_{OH} \times [OH][VOC]. \quad (1)$$

Summation of equation (1) over all VOCs gives the total $RONO_2$ production rate. The largest contribution to the total calculated $RONO_2$ production rate is from C_6–C_{10} alkanes, which were responsible for 80% of the $RONO_2$ production. In the aged DWH plumes, the $RONO_2$ production rate was dominated by oxidation of these long chain alkanes because their mixing ratios (Table 1), $RONO_2$ branching ratios, and k_{OH} [Atkinson *et al.*, 1982; *Roberts*, 1990] were large. The ratio of calculated $RONO_2$ production rates for the sum of C_1–C_{11} $RONO_2$ ($\Sigma RONO_2$) compared to the sum of C_1–C_5 $RONO_2$ is 20. Hence, the measured 60 pptv enhancement in the sum of C_1–C_5 $RONO_2$ in the aged DWH plume (Figure 4b) suggests a greater than 1 ppbv enhancement in $\Sigma RONO_2$. The $\Sigma RONO_2$ calculated from measurements of the parent VOC mixing ratios is consistent with NOy − (NOx + PAN + HNO_3) measured in the aged DWH plume shown in Figure 4b, demonstrating that NOy − (NOx + PAN + HNO_3) accurately represents $\Sigma RONO_2$.

[16] The difference between NOy and (NOx + PAN + HNO_3) increased as the DWH plume aged during downwind transport. Figure 5 shows 1 s measurements of NOy − (NOx + PAN + HNO_3) versus NOy in the MBL over the Gulf of Mexico on 10 June. Many of the gray points with minimal NOy − (NOx + PAN + HNO_3) and increased O_3 were obtained in the northern portion of the flight shown in Figure 1, where air masses with continental origins were sampled. These measurements outside the DWH plume demonstrate that NOx + PAN + HNO_3 usually accounted for the majority of NOy, and that O_3 was not ordinarily correlated with NOy − (NOx + PAN + HNO_3). Similarly, only small differences between NOy and (NOx + PAN + HNO_3) have been reported in other environments, demonstrating that (NOx + PAN + HNO_3) accounted for most of NOy elsewhere (discussed in section 3.4). The slopes of linear least squares fits to the plume data have high correlation coefficients, with r^2 ranging from 0.93 to 0.99. The $\Sigma RONO_2$ fraction of plume NOy is inferred from NOy − (NOx + PAN + HNO_3) versus NOy correlation slopes. $\Sigma RONO_2$/NOy enhancement ratios measured in plume transects increased monotonically with distance from 10 to 50 km downwind from DWH, rising from 0.15 (red line in Figure 5a) to 0.78 (black line in Figure 5a). Substantial $RONO_2$ production in the DWH plume confirms that oxidation of heavier alkanes dominated the NOx-VOC chemistry.

3.6. Photochemical Ozone Production

[17] The elevated alkane concentrations in the DWH plumes led to rapid O_3 formation, but radical termination by $RONO_2$ formation limited the O_3 yield. Comparing calculated to observed O_3 production rates in the DWH plume identifies the processes responsible for O_3 formation. Although O_3 and $RONO_2$ production rate calculation

requires knowledge of OH, which was not measured from the aircraft, the ratio of O_3 to $RONO_2$ production is independent of OH. Reactions of RO_2 with NO produce both O_3 (reaction 2) and $RONO_2$ (reaction 3) [*Roberts*, 1990];

$$NO + RO_2 \rightarrow NO_2 + RO \rightarrow O_3 + NO + RO(\text{with sunlight and } O_2) \quad (2)$$

$$NO + RO_2 \rightarrow RONO_2, \quad (3)$$

where R is an alkyl group and RO is an alkoxy radical. Thus, $RONO_2$ and O_3 production rates are related by the branching between $RONO_2$ formation (which terminates O_3 production) and NO_2 formation (which leads to O_3 production and NO regeneration, thus continuing O_3 production). Since reaction of RO_2 with NO is rapid compared to RO_2 formation from reaction of OH with VOCs, the $RONO_2$ production rate from an individual VOC is given by equation (1), and the O_3 production rate (P_{O_3}) is given by

$$P_{O_3} = \gamma \times (1 - \beta) \times k_{OH} \times [OH][VOC], \quad (4)$$

where γ is the number of O_3 molecules formed from reaction 2. Since reaction 2 usually leads to one O_3 from NO_2 photolysis and another from subsequent reactions of RO, γ is approximately 2. Total O_3 and $RONO_2$ production rates from a VOC mixture are obtained by summing the production rates given by equations (1) and (4) for each VOC. Using equations (1) and (4) with k_{OH} and β from *Perring et al.* [2010], the ratio P_{O_3}/P_{RONO_2} is calculated from measured parent VOC concentrations. Assuming that VOC measurement inaccuracy of ±10% dominates the uncertainties in equations (1) and (4), then summing the two equations over the average VOC speciation in the DWH plume [*Ryerson et al.*, 2011] gives $P_{O_3}/P_{RONO_2} = 8.0 \pm 0.8$.

[18] P_{O_3}/P_{RONO_2} also can be determined from O_3 and $RONO_2$ measurements in the DWH plume and compared to the above value to test if the calculations accurately represent the chemistry. Since O_3 and $RONO_2$ have a common source and negligible depositional or photochemical losses [*Talukdar et al.*, 1997] on the short time scales here, the observed O_3 to $\Sigma RONO_2$ enhancement ratio in the DWH plume is equivalent to the ratio of their production rates. Figure 5b shows 1-s measurements of O_3 (represented by $O_3 + NO_2$ to account for titration of O_3 by NO) versus $\Sigma RONO_2$ (inferred from the difference between measured NOy and (NOx + PAN + HNO_3)). Over the Gulf of Mexico and outside the DWH plume (gray dots in Figure 5b), $\Sigma RONO_2$ determined from NOy − (NOx + PAN + HNO_3) averaged -0.02 ± 0.18 ppbv and was uncorrelated with O_3. Four DWH plume transects are colored as in Figures 1 and 5a. P_{O3}/P_{RONO2} is inferred from the correlation slope of linear least squares fits of O_3 to $\Sigma RONO_2$ observed in each plume transect. O_3 and $\Sigma RONO_2$ were enhanced and highly correlated in the DWH plume transects, with r^2 values ranging from 0.87 to 0.99. In the earliest plume transect 0.5 h downwind, the O_3 to $RONO_2$ correlation slope was 6.2 ± 0.5 (red line in Figure 5b), and the slope rapidly increased to 7.5 ± 0.4 in transects 20–50 km downwind. Within the measurement uncertainties, this observed ratio of production rates agrees with the calculated P_{O_3}/P_{RONO_2} (blue dashed line in Figure 5b) demonstrating that OH oxidation of the measured VOCs accurately describes the O_3 photochemistry and $RONO_2$ production in the DWH plume.

4. Discussion and Conclusions

[19] The release of gas and oil from the deep ocean resulted in a unique atmospheric VOC mixture that allowed O_3 photochemistry from alkanes to be studied in isolation from reactions of other VOCs. The effective branching ratio for production of $RONO_2$ depends on the VOC composition and characterizes the NOx-VOC chemistry that produces O_3. Effective branching ratio determinations are valuable for predicting changes in O_3 formation in response to VOC reductions [*Farmer et al.*, 2011]. By combining equations (1) and (4) and considering all VOCs,

$$P_{O_3}/P_{RONO_2} = \gamma(1 - \beta_e)/\beta_e, \quad (5)$$

where β_e is the effective branching ratio of the entire VOC mixture. Both observed O_3 to $\Sigma RONO_2$ ratios and production rate calculations using measured VOCs determine $\beta_e = 0.2$ in the DWH plume. β_e was considerably higher here than in urban and rural environments, where effective branching ratios ranged from 0.03 to 0.10 [*Farmer et al.*, 2011; *Perring et al.*, 2010]. $RONO_2$ branching ratios increase with n-alkane carbon number [*Atkinson et al.*, 1982; *Roberts*, 1990], and large straight-chain alkanes have branching ratios as high as 0.47 for n-decane. In the DWH plume, C_5–C_{10} alkanes dominated the VOC mixture making β_e uncommonly large. The relatively large β_e in the DWH plume shifted the NOx-VOC chemistry toward $RONO_2$ production, at the expense of O_3 formation.

[20] Ozone production efficiency (OPE), which can be determined observationally from the ratio of O_3 to NOx oxidation products, is used regularly as a metric to assess O_3 photochemistry [e.g., *Trainer et al.*, 1993; *Neuman et al.*, 2009]. The difference NOy−NOx represents the sum of all NOx oxidation products. Since NOy was effectively conserved on the short time scales studied here (≤2.5 h), we interpret the correlation slope from linear least squares fits of measured O_3 to NOy−NOx as net OPE. In the DWH plume, OPE was 6.0 ± 0.5 ppbv/ppbv after 1 h of transport (Figure 3b), and similar to values measured in U.S. urban areas [*Trainer et al.*, 1995; *Neuman et al.*, 2009]. In contrast, petrochemical plumes with OH loss rates dominated by alkenes had OPEs ranging from 10 to 18 [*Ryerson et al.*, 2003] (Figure 3b). On 10 June, O_3 enhancements in the DWH plumes were less than 15 ppbv (Figure 5b), even after NOx was completely oxidized. Although the ratio of VOC to NOx was very large, O_3 production was limited by OH oxidation of C_5–C_{10} alkanes that preferentially formed $RONO_2$ and by NOx levels less than 10 ppbv.

[21] Reactive nitrogen partitioning indicates that O_3 production had effectively ceased in the plumes observed 50 km downwind. NOx had been nearly completely oxidized, and there was little PAN formation that could catalyze later O_3 production. NOx oxidation in the atmospheric DWH plume favored $RONO_2$ production, and approximately 1 h after emission, reactive nitrogen was dominated by $RONO_2$. Since the $RONO_2$ species have photochemical lifetimes of many days [*Talukdar et al.*, 1997] and do not readily

decompose to release NOx, their formation represents a terminating step in NOx-VOC photochemistry on short time scales. The nearly constant relationship between O_3 and $RONO_2$ (inferred from the difference between NOy and individually measured compounds) in plumes aged between 1 and 2.5 h (Figure 5b) confirms that net O_3 production terminated once $RONO_2$ were formed and that $RONO_2$ were not removed rapidly from the atmosphere. The fate of these $RONO_2$ in the atmosphere is slow decomposition by reaction with OH or photolysis over many days or weeks [*Roberts*, 1990; *Kames and Schurath*, 1992; *Clemitshaw et al.*, 1997; *Talukdar et al.*, 1997].

[22] VOCs were considerably more abundant than NOx in the DWH plume and were still substantially enhanced after NOx was depleted. For example, during the 0.5 h transport time between transects 10 and 20 km downwind, n-heptane remained nearly constant and over 15 ppbv, whereas NOx decreased from 7 to 2 ppbv. Although O_3 formation had ceased after NOx was oxidized, efficient plume transport of VOCs from DWH to regions with additional NOx emissions (over land, for example) may initiate further O_3 formation. The measurements and calculations presented here reveal the gas-phase photochemical processes and the resulting secondary reaction products in the DWH plume, and demonstrate that NOx-VOC chemistry in this unique atmospheric VOC mixture is explained by known mechanisms.

[23] **Acknowledgments.** We thank the NOAA Climate Change, Health of the Atmosphere Program for support and the NOAA Aircraft Operation Center staff for accomplishing the Gulf flights.

References

Arey, J., S. M. Aschmann, E. S. C. Kwok, and R. Atkinson (2001), Alkyl nitrate, hydroxyalkyl nitrate, and hydroxycarbonyl formation from the NOx-air photooxidations of C_5–C_8 n-alkanes, *J. Phys. Chem. A*, *105*, 1020–1027, doi:10.1021/jp003292z.

Atkinson, R., S. M. Aschmann, W. P. L. Carter, A. M. Winer, and J. N. Pitts Jr. (1982), Alkyl nitrate formation from the NOx-air photooxidations of C_2–C_8 n-alkanes, *J. Phys. Chem.*, *86*, 4563–4569, doi:10.1021/j100220a022.

Baker, A. K., A. J. Beyersdorf, L. A. Doezem, A. Katzenstein, S. Meinardi, I. J. Simpson, D. R. Blake, and F. S. Rowland (2008), Measurements of nonmethane hydrocarbons in 28 United States cities, *Atmos. Environ.*, *42*, 170–182, doi:10.1016/j.atmosenv.2007.09.007.

Carter, W. P. L. (1994), Development of ozone reactivity scales for volatile organic compounds, *J. Air Waste Manage. Assoc.*, *44*, 881–899.

Chen, H., et al. (2010), High-accuracy continuous airborne measurements of greenhouse gases (CO_2 and CH_4) using the cavity ring-down spectroscopy (CRDS) technique, *Atmos. Meas. Tech.*, *3*(2), 375–386, doi:10.5194/amt-3-375-2010.

Clemitshaw, K. C., J. Williams, O. V. Rattigan, D. E. Shallcross, K. S. Law, and R. A. Cox (1997), Gas-phase ultraviolet absorption cross-sections and atmospheric lifetimes of several C_2-C_5 alkyl nitrates, *J. Photochem. Photobiol. A*, *102*, 117–126, doi:10.1016/S1010-6030(96)04458-9.

Colman, J. J., A. L. Swanson, S. Meinardi, B. Sive, D. R. Blake, and F. S. Rowland (2001), Description of the analysis of a wide range of volatile organic compounds in whole air samples collected during PEM-Tropics A and B, *Anal. Chem.*, *73*, 3723–3731, doi:10.1021/ac010027g.

Day, D. A., M. B. Dillon, P. J. Wooldridge, J. A. Thornton, R. S. Rosen, E. C. Wood, and R. C. Cohen (2003), On alkyl nitrates, O_3, and the "missing NO_y," *J. Geophys. Res.*, *108*(D16), 4501, doi:10.1029/2003JD003685.

de Gouw, J. A., et al. (2011), Organic aerosol formation downwind from the Deepwater Horizon oil spill, *Science*, *331*, 1295–1299, doi:10.1126/science.1200320.

Fahey, D. W., G. Hubler, D. D. Parrish, E. J. Williams, R. B. Norton, B. A. Ridley, H. B. Singh, S. C. Liu, and F. C. Fehsenfeld (1986), Reactive nitrogen species in the troposphere: Measurements of NO, NO_2, HNO_3, particulate nitrate, peroxyacetyl nitrate (PAN), O_3, and total reactive odd nitrogen (NO_y) at Niwot Ridge, Colorado, *J. Geophys. Res.*, *91*(D9), 9781–9793, doi:10.1029/JD091iD09p09781.

Farmer, D. K., et al. (2011), Impact of organic nitrates on urban ozone production, *Atmos. Chem. Phys.*, *11*, 4085–4094, doi:10.5194/acp-11-4085-2011.

Flocke, F., A. Volz-Thomas, H.-J. Buers, W. Pätz, H.-J. Garthe, and D. Kley (1998), Long-term measurements of alkyl nitrates in southern Germany: 1. General behavior and seasonal and diurnal variation, *J. Geophys. Res.*, *103*, 5729–5746, doi:10.1029/97JD03461.

Gilman, J. B., et al. (2009), Measurements of volatile organic compounds during the 2006 TexAQS/GoMACCS campaign: Industrial influences, regional characteristics, and diurnal dependencies of the OH reactivity, *J. Geophys. Res.*, *114*, D00F06, doi:10.1029/2008JD011525.

Holloway, J. S., R. O. Jakoubek, D. D. Parrish, C. Gerbig, A. Volz-Thomas, S. Schmitgen, A. Fried, B. Wert, B. Henry, and J. R. Drummond (2000), Airborne intercomparison of vacuum ultraviolet fluorescence and tunable diode laser absorption measurements of tropospheric carbon monoxide, *J. Geophys. Res.*, *105*, 24,251–24,261, doi:10.1029/2000JD900237.

Jobson, B. T., C. M. Berkowitz, W. C. Kuster, P. D. Goldan, E. J. Williams, F. C. Fehsenfeld, E. C. Apel, T. Karl, W. A. Lonneman, and D. Riemer (2004), Hydrocarbon source signatures in Houston, Texas: Influence of the petrochemical industry, *J. Geophys. Res.*, *109*, D24305, doi:10.1029/2004JD004887.

Kames, J., and U. Schurath (1992), Alkyl nitrates and bifunctional nitrates of atmospheric interest: Henry's Law constants and their temperature dependencies, *J. Atmos. Chem.*, *15*, 79–95, doi:10.1007/BF00053611.

Madronich, S. (2006), Chemical evolution of gaseous air pollutants downwind of tropical megacities: Mexico City case study, *Atmos. Environ.*, *40*, 6012–6018, doi:10.1016/j.atmosenv.2005.08.047.

National Research Council Committee on Tropospheric Ozone Formation and Measurement (1991), *Rethinking the Ozone Problem in Urban and Regional Air Pollution*, Natl. Acad. Press, Washington, D. C.

Neuman, J. A., et al. (2002), Fast-response airborne in situ measurements of HNO_3 during the Texas 2000 Air Quality Study, *J. Geophys. Res.*, *107*(D20), 4436, doi:10.1029/2001JD001437.

Neuman, J. A., et al. (2006), Reactive nitrogen transport and photochemistry in urban plumes over the North Atlantic Ocean, *J. Geophys. Res.*, *111*, D23S54, doi:10.1029/2005JD007010.

Neuman, J. A., et al. (2009), Relationship between photochemical ozone production and NO_x oxidation in Houston, Texas, *J. Geophys. Res.*, *114*, D00F08, doi:10.1029/2008JD011688.

O'Brien, J. M., P. B. Shepson, Q. Wu, T. Biesenthal, J. W. Bottenheim, H. A. Wiebe, K. G. Anlauf, and P. Brickell (1997), Production and distribution of organic nitrates, and their relationship to carbonyl compounds in an urban environment, *Atmos. Environ.*, *31*(14), 2059–2069, doi:10.1016/S1352-2310(97)80002-7.

Parrish, D. D., et al. (1993), The total reactive oxidized nitrogen levels and the partitioning between the individual species at six rural sites in eastern North America, *J. Geophys. Res.*, *98*(D2), 2927–2939, doi:10.1029/92JD02384.

Perring, A. E., et al. (2010), The production and persistence of $\Sigma RONO_2$ in the Mexico City plume, *Atmos. Chem. Phys.*, *10*, 7215–7229, doi:10.5194/acp-10-7215-2010.

Pollack, I. B., B. M. Lerner, and T. B. Ryerson (2011), Evaluation of ultraviolet light-emitting diodes for detection of atmospheric NO_2 by photolysis - chemiluminescence, *J. Atmos. Chem.*, *65*(2), 111–125, doi:10.1007/s10874-011-9184-3.

Reeves, C. E., et al. (2007), Alkyl nitrates in outflow from North America over the North Atlantic during Intercontinental Transport of Ozone and Precursors 2004, *J. Geophys. Res.*, *112*, D10S37, doi:10.1029/2006JD007567.

Roberts, J. M. (1990), The atmospheric chemistry of organic nitrates, *Atmos. Environ., Part A*, *24*, 243–287.

Ryerson, T. B., et al. (1998), Emission lifetimes and ozone formation in power plant plumes, *J. Geophys. Res.*, *103*, 22,569–22,583, doi:10.1029/98JD01620.

Ryerson, T. B., L. G. Huey, K. Knapp, J. A. Neuman, D. D. Parish, D. T. Sueper, and F. C. Fehsenfeld (1999), Design and initial characterization of an inlet for gas-phase NO_y measurements from aircraft, *J. Geophys. Res.*, *104*, 5483–5492, doi:10.1029/1998JD100087.

Ryerson, T. B., et al. (2003), Effect of petrochemical industrial emissions of reactive alkenes and NO_x on tropospheric ozone formation in Houston, Texas, *J. Geophys. Res.*, *108*(D8), 4249, doi:10.1029/2002JD003070.

Ryerson, T. B., et al. (2011), Atmospheric emissions from the Deepwater Horizon spill constrain air-water partitioning, hydrocarbon fate, and leak rate, *Geophys. Res. Lett.*, *38*, L07803, doi:10.1029/2011GL046726.

Schneider, M., O. Luxenhofer, A. Deissler, and K. Ballschmiter (1998), C_1–C_{15} alkyl nitrates, benzyl nitrate, and bifunctional nitrates: Measurements in California and South Atlantic air and global comparison using C_2Cl_4 and $CHBr_3$ as marker molecules, *Environ. Sci. Technol.*, *32*(20), 3055–3062, doi:10.1021/es980132g.

Simpson, I. J., N. J. Blake, D. R. Blake, E. Atlas, F. Flocke, J. H. Crawford, H. E. Fuelberg, C. M. Kiley, S. Meinardi, and F. S. Rowland (2003), Photochemical production and evolution of selected C_2–C_5 alkyl nitrates in tropospheric air influenced by Asian outflow, *J. Geophys. Res.*, *108*(D20), 8808, doi:10.1029/2002JD002830.

Simpson, I. J., T. Wang, H. Guo, Y. H. Kwok, F. Flocke, E. Atlas, S. Meinardi, F. S. Rowland, and D. R. Blake (2006), Long-term atmospheric measurements of C_1–C_5 alkyl nitrates in the Pearl River Delta region of southeast China, *Atmos. Environ.*, *40*, 1619–1632, doi:10.1016/j.atmosenv.2005.10.062.

Slusher, D. L., L. G. Huey, D. J. Tanner, F. M. Flocke, and J. M. Roberts (2004), A thermal dissociation-chemical ionization mass spectrometry (TD-CIMS) technique for the simultaneous measurement of peroxyacylnitrates and dinitrogen pentoxide, *J. Geophys. Res.*, *109*, D19315, doi:10.1029/2004JD004670.

Talbot, R., et al. (2003), Reactive nitrogen in Asian continental outflow over the western Pacific: Results from the NASA Transport and Chemical Evolution over the Pacific (TRACE-P) airborne mission, *J. Geophys. Res.*, *108*(D20), 8803, doi:10.1029/2002JD003129.

Talukdar, R. K., J. B. Burkholder, M. Hunter, M. K. Gilles, J. M. Roberts, and A. R. Ravishankara (1997), Atmospheric fate of several alkyl nitrates, *J. Chem. Soc. Faraday Trans.*, *93*(16), 2797–2805, doi:10.1039/a701781b.

Trainer, M., et al. (1993), Correlation of ozone with NO_y in photochemically aged air, *J. Geophys. Res.*, *98*, 2917–2925, doi:10.1029/92JD01910.

Trainer, M., B. A. Ridley, M. P. Buhr, G. Kok, J. Walega, G. Hübler, D. D. Parrish, and F. C. Fehsenfeld (1995), Regional ozone and urban plumes in the southeastern United States: Birmingham, a case study, *J. Geophys. Res.*, *100*, 18,823–18,834, doi:10.1029/95JD01641.

Washenfelder, R. A., et al. (2010), Characterization of NOx, SO_2, ethene, and propene from industrial emission sources in Houston, Texas, *J. Geophys. Res.*, *115*, D16311, doi:10.1029/2009JD013645.

Worton, D. R., et al. (2010), Alkyl nitrate photochemistry during the tropospheric organic chemistry experiment, *Atmos. Environ.*, *44*, 773–785, doi:10.1016/j.atmosenv.2009.11.038.

Yvon-Lewis, S. A., L. Hu, and J. Kessler (2011), Methane flux to the atmosphere from the Deepwater Horizon oil disaster, *Geophys. Res. Lett.*, *38*, L01602, doi:10.1029/2010GL045928.